Int. J. Heat Mass Transfer. Vol. 25, No. 8, pp. 1167–1181, 1982
Printed in Great Britain

0017–9310/82/081167–15 $03.00/0
Pergamon Press Ltd.

THE EFFECT OF TURBULENCE PROMOTERS ON MASS TRANSFER—NUMERICAL ANALYSIS AND FLOW VISUALIZATION

IN SEOK KANG and HO NAM CHANG*
Department of Chemical Engineering, Korea Advanced Institute of Science and Technology, P.O. Box 150, Chongyangni, Seoul, Korea

(*Received* 2 *July* 1980 *and in final form* 13 *January* 1982)

Abstract—Numerical investigations are made on mass transfer in a 2-dim. flow between two parallel plates with turbulence promoters fixed to the lower and/or the upper walls. The 'zigzag-type' and 'cavity-type' geometries are used, for which mass transfer and flow visualization studies are conducted in the laminar flow regime. The numerical results show that turbulence promoters enhance the mass transfer by forming a recirculating flow which causes a convective mass transfer effect and increases the wall shear stress in the main stream.

The flow separations observed by visualization studies are in good agreement with the predictions made by the numerical analysis at Reynolds numbers ranging from 20 to 150. Also the visualization shows that the unsteady flow in the channel begins at Reynolds numbers of 250–300 for both geometries with the aspect ratio of 5.

NOMENCLATURE

A, aspect ratio, $\Delta L/H$;
C, concentration;
$C_{S,max}$, maximum concentration at the inlet plane S;
c, dimensionless concentration, $C/C_{S,max}$;
D_{eff}, effective diffusion coefficient;
H, height of the channel;
Δh, grid size, y-direction;
K, a proportionality constant used for the correlation of $Sh(Re, Sc)$;
ΔL, distance between the centers of two neighboring promoters;
n, dimensionless coordinate normal to the wall used in equation (9);
u, dimensionless velocity component, x-direction;
V, volume-averaged velocity;
X, Y, X-, Y-coordinates;
x, y, X/H, Y/H, dimensionless coordinates.

Greek symbols

ρ, density of the fluid;
ψ, dimensionless stream function;
ω, dimensionless vorticity;
φ, general dependent variable;
μ, viscosity of the fluid.

Dimensionless groups

Pe, Peclet number $(Re \cdot Sc)$, VH/D_{eff};
Re, Reynolds number, $V\rho H/\mu$;
Sc, Schmidt number, $\mu/\rho D_{eff}$;
Sh_x, local Sherwood number, $\left.\frac{\partial c}{\partial y}\right|_{y=0}$ or $-\left.\frac{\partial c}{\partial y}\right|_{y=1}$;
Sh, Sh_m, mean Sherwood number, $\frac{1}{2(A-2)}\int_1^{A-1}(Sh_{x,y=0}+Sh_{x,y=1})\,dx$;

Subscripts and superscripts

S, S′, T, T′, corresponding planes of the modelled promoters;
S, max, maximum value on the plane S;
S′, max maximum value on the plane S′;
(n), nth cycle of iteration.

*To whom all correspondence should be addressed.

1. INTRODUCTION

THE TURBULENCE promoter is one of several devices employed for enhancing the mass transfer efficiency of processes having high Peclet numbers, such as electrodialysis and artificial kidney systems. Many workers have investigated the effects of promoters owing to their importance to the mass transfer effects of the electrodialysis system and their experimental results have been summarized [1]. Belfort and Guter [2] discuss the role of hydrodynamics in electrodialysis in order to provide some criteria for the evaluation of promoters. Winograd *et al.* [3] have proposed the mesh step model which represents the mass transfer process as a laminar concentration boundary layer, the development of which is periodically interrupted by turbulence promoters. Recently mass transfer to slightly perturbed walls of a channel has been studied [4–6]. However, most of this work has been limited either to experimental studies or to analyses for simplified flow fields.

On the other hand recirculating flow problems have been examined frequently because of the classical nature of this problem in fluid mechanics. Analytical studies [7–11] have been performed for the limiting cases of this flow and numerical techniques [8, 12–19] have been applied to simple geometries such as rectangular cavities. However there exists no rigorous and systematic treatment of mass transfer in a parallel channel with rectangular promoters where the flow field and mass transfer are considered simultaneously.

In this study the numerical analyses for the two modelled systems of 'zigzag-' and 'cavity-type' geometries are carried out in order to elucidate the flow fields and the mass transfer in the laminar recirculating flow formed by the promoters. Since the thickness of the concentration boundary layer is highly dependent on the hydrodynamic conditions in the channel, the stream functions and dimensionless velocity gradient distributions are analyzed. The local Sherwood number distributions along the channel are evaluated for Reynolds numbers ranging from 50 to 500 and Schmidt numbers from 20 to 2000 to yield the characteristics of the mass transfer. The results are correlated to give Sherwood numbers in the form of $Sh = Sh(Sc, Re)$. Finally flow visualization experiments are used to verify that the numerically obtained streamline distributions are consistent with the experimental findings.

2. MODELLED SYSTEMS AND GOVERNING EQUATIONS

An electrodialyzer with the turbulence promoters is shown schematically in Fig. 1. The steady-state mass transfer in this system can be treated as a 2-dim. problem with the simplifying assumption that the width is much larger than the height of the channel ($W/H \gg 1$). Figure 2 shows the two types of the turbulence promoters considered in the present study. Model I is called the 'zigzag-type' promoter and has all promoters on the lower and the upper walls of the channel in an alternating fashion. In contrast to Model I, the promoters in Model II, called 'cavity-type' promoter, are equally spaced along the lower wall. The height of the promoter is exactly one half that of the channel. All coordinates (rectangular) and boundary conditions are described in dimensionless form.

The problem to be solved can be described by the following three dimensionless equations, namely the stream function equation, the vorticity transport equation and the mass transfer equation [20, 21]:

$$\nabla^2\psi = -\omega, \tag{1}$$

$$\nabla^2\omega = Re\left(\frac{\partial\psi}{\partial y}\frac{\partial\omega}{\partial x} - \frac{\partial\psi}{\partial x}\frac{\partial\omega}{\partial y}\right), \tag{2}$$

$$\nabla^2 c = Pe\left(\frac{\partial\psi}{\partial y}\frac{\partial c}{\partial x} - \frac{\partial\psi}{\partial x}\frac{\partial c}{\partial y}\right). \tag{3}$$

The local change in concentration is assumed not to cause any disturbances in the fluid motion. For fluid motion a no-slip condition is used at the surfaces of the promoters and at the walls of the channel under consideration. For mass transfer the high polarization limit and no-flux boundary conditions are chosen at the fluid–channel wall interface and the surfaces of the promoters, respectively. Then the conditions for the flow fields are

at the upper walls

$$\psi = 1, \quad \frac{\partial\psi}{\partial x} = \frac{\partial\psi}{\partial y} = 0, \tag{4}$$

at the lower walls

$$\psi = 0, \quad \frac{\partial\psi}{\partial x} = \frac{\partial\psi}{\partial y} = 0. \tag{5}$$

The conditions for the concentration profile are

at conducting walls $\quad c = 0$ (6)

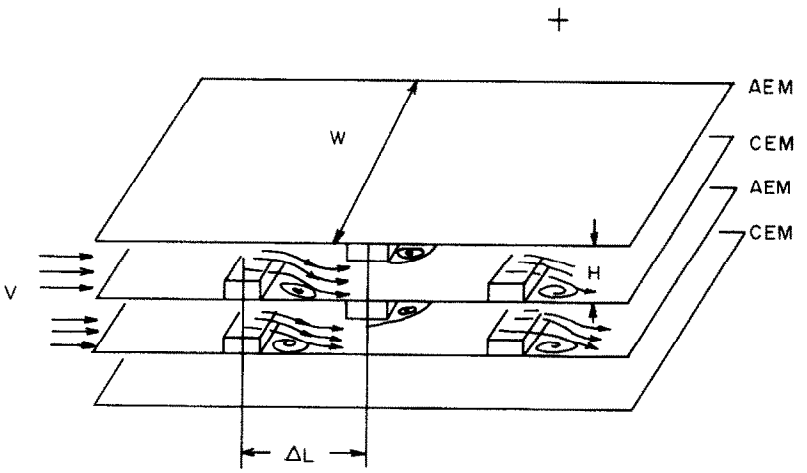

FIG. 1. Schematic diagram of an electrodialyzer with turbulence promoters: AEM, anion exchange membrane; CEM, cation exchange membrane.

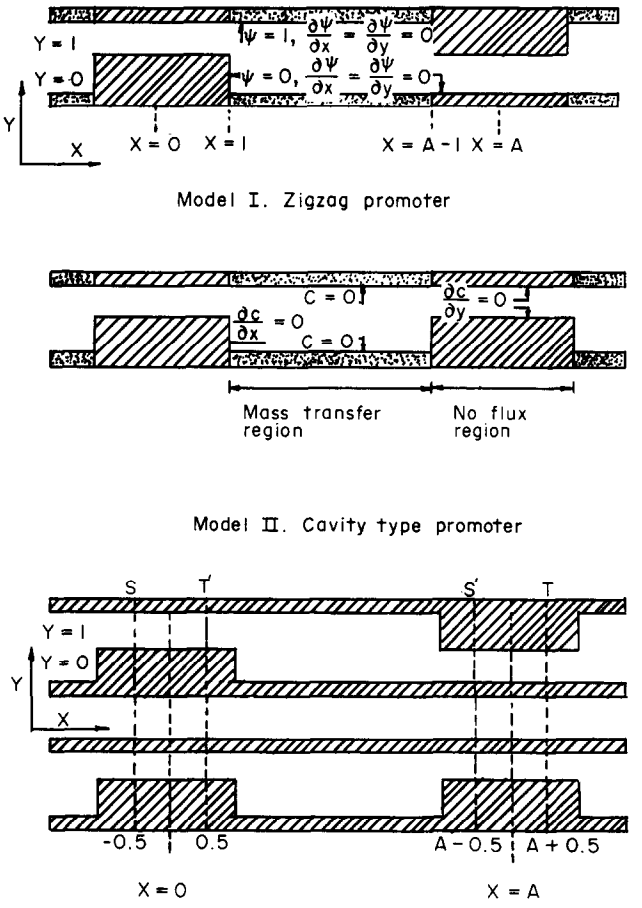

FIG. 2. Modelled systems for turbulence promoters.

at non-conducting walls $\frac{\partial c}{\partial x} = 0$ or $\frac{\partial c}{\partial y} = 0.$ (7)

In addition to the above boundary conditions we have assumed the fully developed concentration profile normalized with respect to C_{max} in each promoter unit. In other words the flow field and the concentration profile in each promoter unit look like those of the preceding unit. Then the boundary values at the inlet and the outlet of one unit can be calculated using Mitchell's method [22]. In order to use Mitchell's method two pairs of corresponding planes, (S, S') and (T, T') are assigned as shown in Fig. 2. The values calculated in the numerical procedure at S' and T' should be used at the end of each iteration to update the values at S and T. The relations between the former and the latter planes are as follows for the flow fields:

zigzag-type promoter

$$\psi_S(y) = 1 - \psi_{S'}(1 - y),\ \psi_T(y) = 1 - \psi_{T'}(1 - y),$$
$$\omega_S(y) = -\omega_{S'}(1 - y),\ \omega_T(y) = -\omega_{T'}(1 - y), \quad (8)$$

cavity-type promoter

$$\psi_S(y) = \psi_{S'}(y),\quad \psi_T(y) = \psi_{T'}(y),$$
$$\omega_S(y) = \omega_{S'}(y),\quad \omega_T(y) = \omega_{T'}(y). \quad (9)$$

In equation (3) the dimensionless concentration c is normalized with respect to the maximum concentration at the plane S. That is

$$c_{S,max} = 1. \quad (10)$$

The relations for the concentration profiles are

zigzag-type promoter

$$c_S(y) = c_{S'}(1 - y)/c_{S',max},$$
$$c_T(y) = c_{T'}(1 - y)\cdot c_{S',max}, \quad (11)$$

cavity-type promoter

$$c_S(y) = c_{S'}(y)/c_{S',max},$$
$$c_T(y) = c_{T'}(y)\cdot c_{S',max} \quad (12)$$

where the subscripts are as defined in the Nomenclature.

3. NUMERICAL ANALYSIS

3.1. *Upwind finite difference equation*

The upwind difference scheme developed by Gosman *et al.* [13] for the solutions of the Navier–Stokes equation and the mass transfer equation is used here.

The governing equations in rectangular coordinates can be expressed in the following form:

Table 1. The coefficients of equation (13)

φ	a_φ	b_φ	c_φ	d_φ
ω	1	1	$1/Re$	0
ψ	0	1	1	$-\omega$
c	1	$1/(Re \cdot Sc)$	1	0

$$a_\varphi\left[\frac{\partial}{\partial x}\left(\varphi\frac{\partial\psi}{\partial y}\right)-\frac{\partial}{\partial y}\left(\varphi\frac{\partial\psi}{\partial x}\right)\right]-\frac{\partial}{\partial x}\left[b_\varphi\frac{\partial}{\partial x}(c_\varphi\varphi)\right]+\frac{\partial}{\partial y}\left[b_\varphi\frac{\partial}{\partial y}(c_\varphi\varphi)\right]+d_\varphi=0 \quad (13)$$

in which φ represents the dependent variables (stream function, vorticity, concentration, etc.), ψ is the stream function and a_φ, b_φ, c_φ, d_φ are the coefficients. The coefficients for the present system are listed in Table 1.

The vorticity at the wall is approximated with the assumption that vorticity varies linearly from the wall to the neighbouring point instead of the common uniform vorticity approximation [13], that is

$$\omega_P=-\left[\frac{3(\psi_{NP}-\psi_P)}{n_{NP}^2}+\frac{\omega_{NP}}{2}\right] \quad (14)$$

where the subscript NP denotes the neighbouring point and n_{NP} represents the normal distance from the point P on the wall to the point NP.

3.2. *Numerical procedure*

The system parameters for the simulation of the process are chosen such that the real mass transfer process in electrodialysis is taken into account in the range of laminar flows. The values are as follows:

aspect ratio 3.5, 5,
Reynolds number 50, 100, 200, 500,
Schmidt number 20, 60, 200, 600, 2000.

Non-uniform grid nodes (67 × 21) are chosen in order to account for the concentration boundary layer. The mesh size ranges from $\Delta h = 1/200$ to $\Delta h = 1/10$. The smallest mesh size 1/200 near the wall is designed in consideration of the thickness of the concentration boundary layer. The x, y values on the grid nodes are listed in Table 2. In order to test the effects of false diffusion, the total number of nodes is increased to 67 × 31 ($\Delta h = 3/1000$ to $\Delta h = 1/20$) for some Reynolds numbers and Schmidt numbers. As the convergence criterion, the absolute maximum in the field is adopted as

$$|\varphi^{(n)}-\varphi^{(n-1)}|_{max}<10^{-5}. \quad (15)$$

Relaxation is carried out using

$$\varphi^{(n)}=(1-RP)\varphi^{(n-1)}+RP\bar{\varphi}^{(n)} \quad (16)$$

in which $\bar{\varphi}^{(n)}$ is the value calculated by equation (13) and represents the revised value for the nth cycle of the iteration. Under-relaxation is adopted here in order to damp out the instability occurring due to the non-uniform grid.

Converged solutions can be obtained by using a relaxation parameter, RP, of 0.7 for the flow field and 0.9 for the concentration profile.

In evaluating local Sherwood numbers at the wall a second-order polynomial was used to approximate the concentration near the wall.

3.3. *Results and discussion of the numerical analysis*

Flow field. The distributions of streamlines for Reynolds numbers $Re = 50$, 100, 200 and 500 for promoters with the aspect ratio $A = 5$ are shown in Fig. 3. In the case of zigzag-type promoters, two eddies are formed: the first is located inside the separated flow enclosed by the upper wall and the second enclosed by the upper wall and the promoter. As the Reynolds number increases, the size of both eddies becomes larger and the center location of the first eddy moves to the right side of the geometric center of the eddy.

For the cavity-type promoter with the aspect ratio $A = 5$, a similar phenomena can be observed at low Reynolds numbers ($Re \leqslant 50$). However, as the Reynolds number increases, the first eddy grows rapidly and the contour $\psi = 0$ becomes detached from the lower wall. In this instance the two eddies coexist under the contour $\psi = 0$ and there exists an interesting region where the circulating direction is changed, i.e. the first eddy turns clockwise and the second eddy turns in the opposite direction ($Re = 100$). The further increase of the Reynolds number results in the obliteration of the second eddy and the center of the first eddy moves downstream rapidly ($Re = 200$, 500).

Table 2. Grid points (the aspect ratio $A = 5$)

x	−0.5	−0.4	−0.3	−0.2	−0.1	0.0	0.1
	0.2	0.3	0.4	0.5	0.6	0.7	0.8
	0.9	0.95	1.0	1.05	1.1	1.15	1.225
	1.3	1.4	1.5	1.6	1.7	1.8	1.9
	2.0	2.1	2.2	2.3	2.4	2.5	2.6
	2.7	2.8	2.9	3.0	3.1	3.2	3.3
	3.4	3.5	3.6	3.7	3.775	3.85	3.9
	3.95	4.0	4.05	4.1	4.2	4.3	4.4
	4.5	4.6	4.7	4.8	4.9	5.0	5.1
	5.2	5.3	5.4	5.5			
y	0.0	0.005	0.015	0.03	0.05	0.1	0.2
	0.3	0.4	0.45	0.5	0.55	0.6	0.7
	0.8	0.9	0.95	0.97	0.985	0.995	1.0

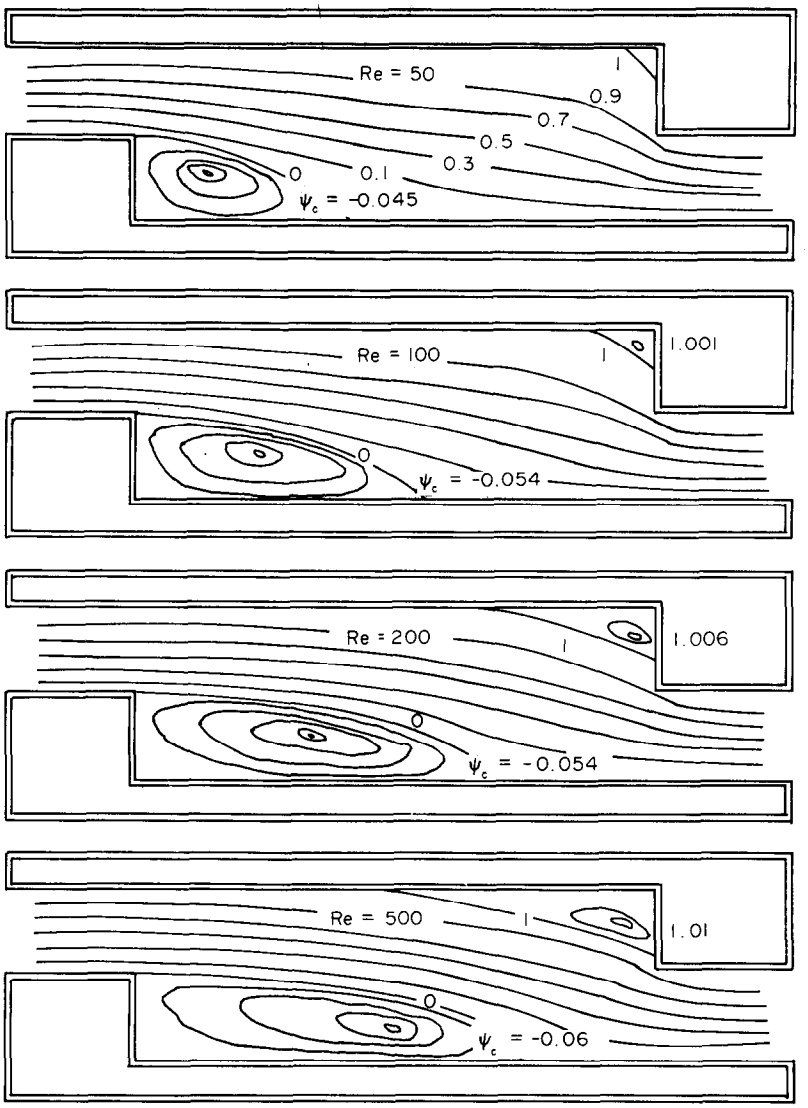

FIG. 3(a). Streamline distributions ($A = 5$) for the zigzag-type promoter.

The shift of the eddy center to the far right side of the cavity can be considered to be different from the problem of cavity flow induced by the uniform translation of the upper wall. However the centers are located at the two-thirds of the cavity depth, which coincides well with the results of Pan and Acrivos [19].

In the system the mass transfer rate at the lower wall depends largely on the dimensionless velocity gradient at $y = 0$ [23, 24]. That is, the larger the velocity gradient, the greater the mass transfer becomes. The dimensionless velocity gradient, $-(\partial u/\partial y)_{y=0}$ at the lower wall of the zigzag-type promoter with the aspect ratio $A = 5$ are plotted for $Re = 50$, 100, 200 and 500 in Fig. 4. It is worthwhile noting that the dimensionless velocity gradient increases as the Reynolds number increases while the dimensionless velocity gradient does not vary with the change of the flow rate in the case of the straight channel. In other words, as the Reynolds number increases the dimensionless shear stress decreases more slowly than that of the straight channel for which the wall shear stress is reciprocally proportional to the Reynolds number. This clearly indicates that the zigzag-type promoter enhances the mass transfer as compared with the straight channel without it. This also implies that the exponent y in $Sh = K\,Sc^x Re^y$ is larger than the calculated value (1/3) of the Reynolds number in a straight channel [21].

Local Sherwood number. The variation of the nondimensional concentration gradient (local Sherwood number) along the upper and lower walls is shown in Fig. 5. The gradient at $x = 1, y = 1$ is only in the region 200–350 instead of, as would be expected, approaching infinity. This is due to the limitation of grid size adopted in the numerical analysis. From Figs. 4 and 5 it can be seen that local Sherwood number distributions are closely related to the dimensionless velocity gradient distributions at the wall and the convective mass transfer in the recirculating flows. The

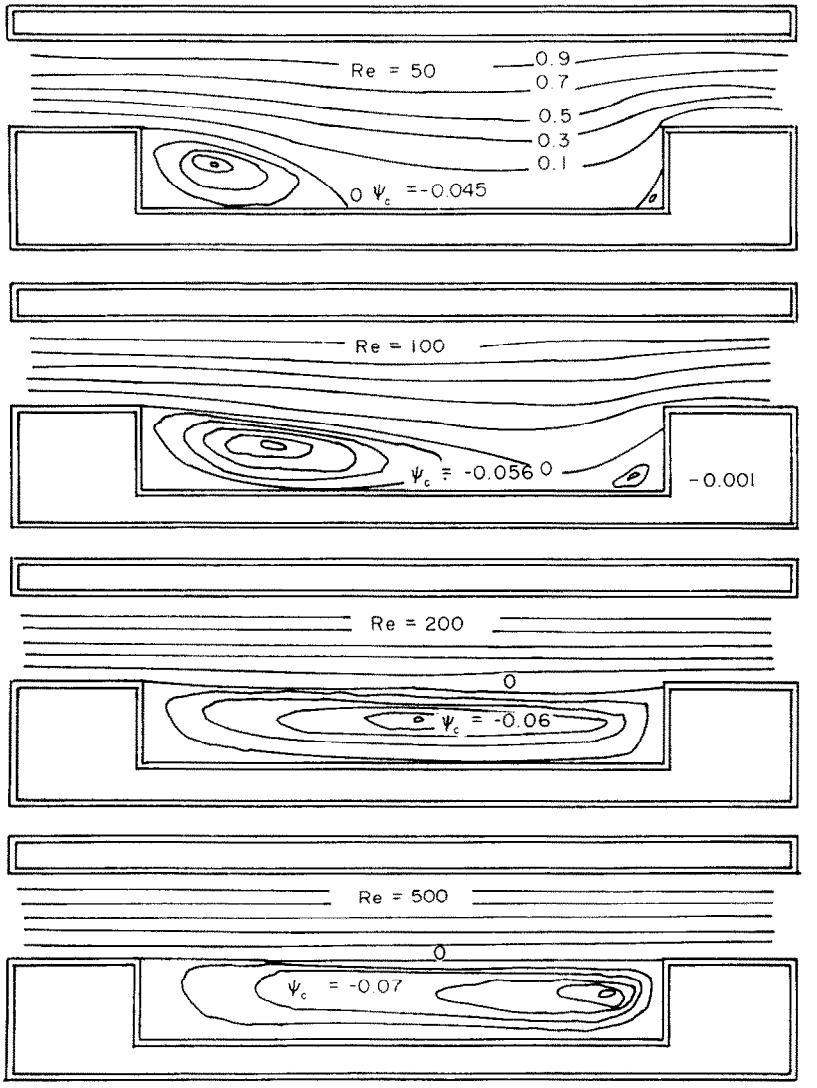

FIG. 3(b). Streamline distributions ($A = 5$) for the cavity-type promoter.

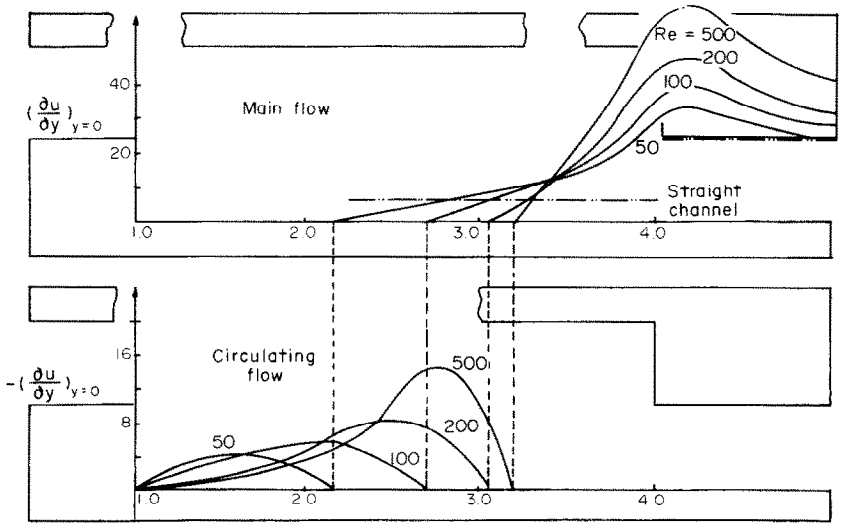

FIG. 4(a). Dimensionless velocity gradient along the lower wall for the zigzag-type promoter.

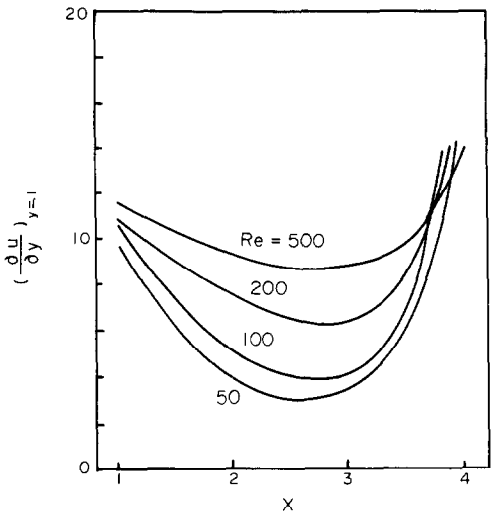

FIG. 4(b). Dimensionless velocity gradient along the upper wall of the cavity-type promoter.

effect of the velocity gradient is illustrated by the curves for the upper walls of the cavity-type promoters. The curves show that the minimum value of the local Sherwood number is located in the vicinity of the point of the minimum velocity gradient. In the case of the upper wall of the zigzag-type promoter, the minimum point is near $x = 4$ for $Re = 200$. These are also the places where the main stream detaches from the wall at the respective Reynolds number.

Mean Sherwood number over one step on promoter. Comparison is made in Table 3 of the performance of zigzag-type and cavity-type promoters. It is evident

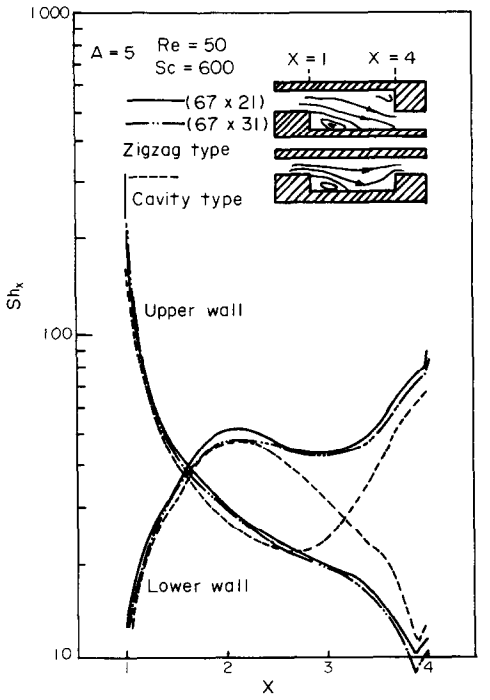

FIG. 5(a). Local Sherwood number distributions ($Re = 50$, $Sc = 600$).

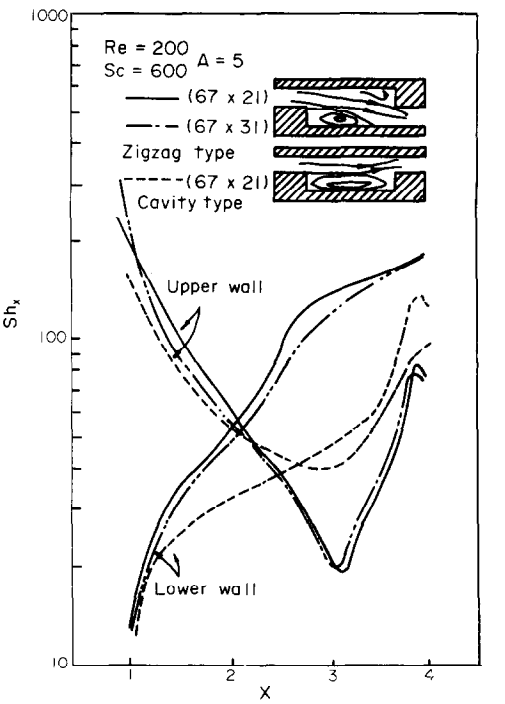

FIG. 5(b). Local Sherwood number distributions ($Re = 200$, $Sc = 600$).

that the zigzag-type is superior to the cavity-type promoter and that the difference in the mean Sherwood numbers becomes larger at higher Reynolds and Schmidt numbers. In order to find any correlation between the Sherwood numbers in terms of the Schmidt and Reynolds numbers for the promoters with the aspect ratio $A = 5$, the mean Sherwood numbers are plotted vs $Sc^x Re^y$ as shown in Fig. 6 after obtaining the x, y values from the logarithmic plot of

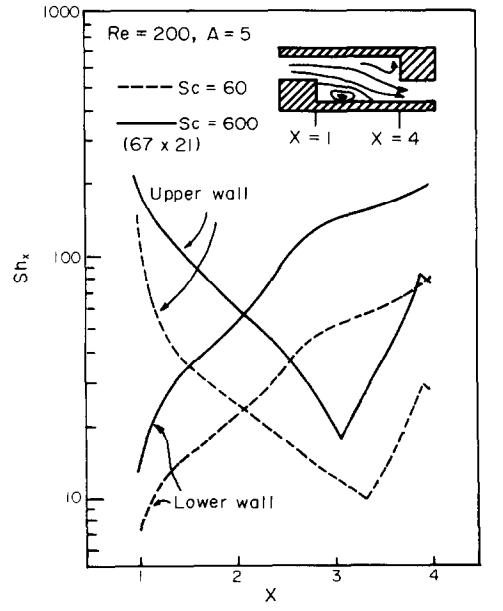

FIG. 5(c). Local Sherwood number distributions ($Re = 200$, $Sc = 60$ and 600).

Table 3. Comparison of the mean Sherwood numbers for each promoter

	Re							
	50		100		200		500	
Sc	zigzag	cavity	zigzag	cavity	zigzag	cavity	zigzag	cavity
20	24.4	22.9	31.9	26.5	42.8	31.0	67.1	37.5
60	35.7	33.3	46.8	38.6	64.3	46.5	104.9	58.3
200	53.9	49.9	72.7	59.2	103.6	73.2	169.3	95.8
600	80.6	73.6	112.7	89.7	160.7	113.7	249.3	151.3
2000	130.8	117.8	182.1	144.6	248.5	185.9	343.1	239.6

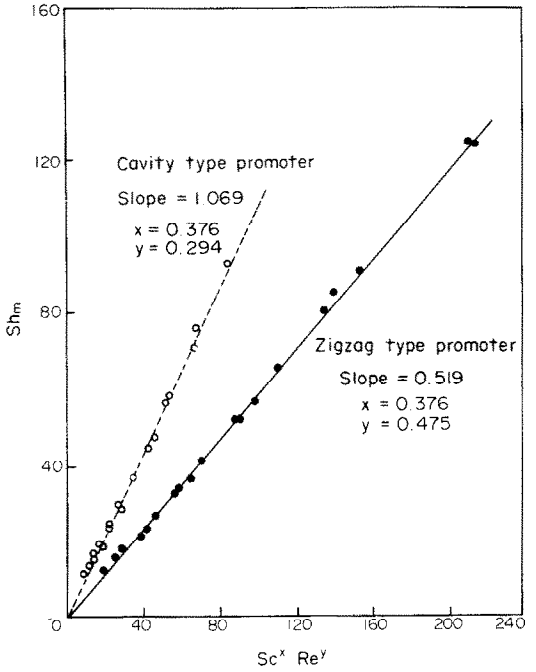

FIG. 6. $Sh = Sh(Sc, Re)$ correlations for the turbulence promoters.

Sh vs *Re* or *Sh* vs *Sc*. The proportionality constants K values are obtained from the slopes of the straight lines in Fig. 6. The values are 0.519 for the zigzag-type promoter and 1.069 for the cavity-type promoter. Thus the correlations can be expressed in the following form:

$$\text{zigzag-type promoter} \quad Sh = 0.519\, Sc^{0.376} Re^{0.475}$$

$$\text{cavity-type promoter} \quad Sh = 1.069\, Sc^{0.376} Re^{0.294}$$

where $10^3 \leqslant Sc \cdot Re \leqslant 4 \times 10^5$.

For another zigzag-type promoter with the aspect ratio $A = 3.5$, the logarithmic plot of *Sh* vs *Re* also gave a straight line for $Sc = 60$. The x value obtained (0.470) is nearly the same as that for the promoter with the aspect ratio $A = 5$ (0.475). This partially indicates that the coefficient K is not a function of the Schmidt number or the Reynolds number but a function of the aspect ratio only.

The effects of false diffusion were tested by varying the total number of nodes from 67 × 21 to 67 × 31. In Fig. 7 the results of the test are presented for the zigzag-type promoter with the aspect ratio $A = 5$ at $Re = 50$ and 200. Although 67 × 31 grid nodes give mean Sherwood numbers slightly less than those obtained

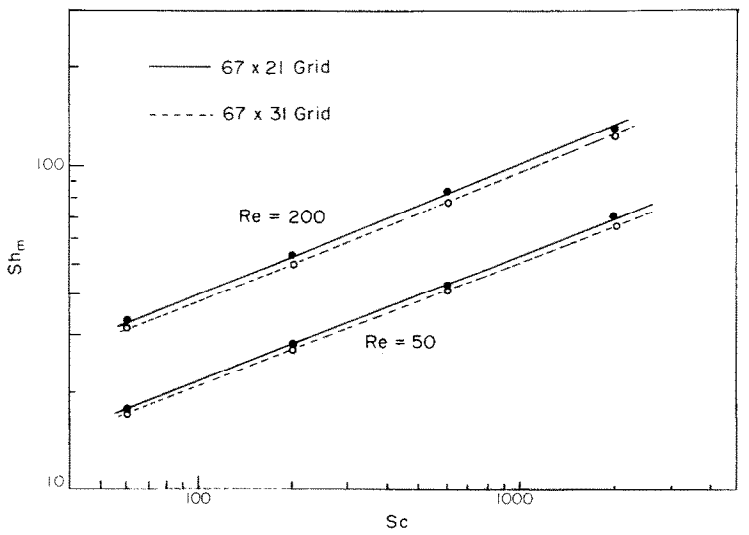

FIG. 7. The effect of false diffusion on the solution.

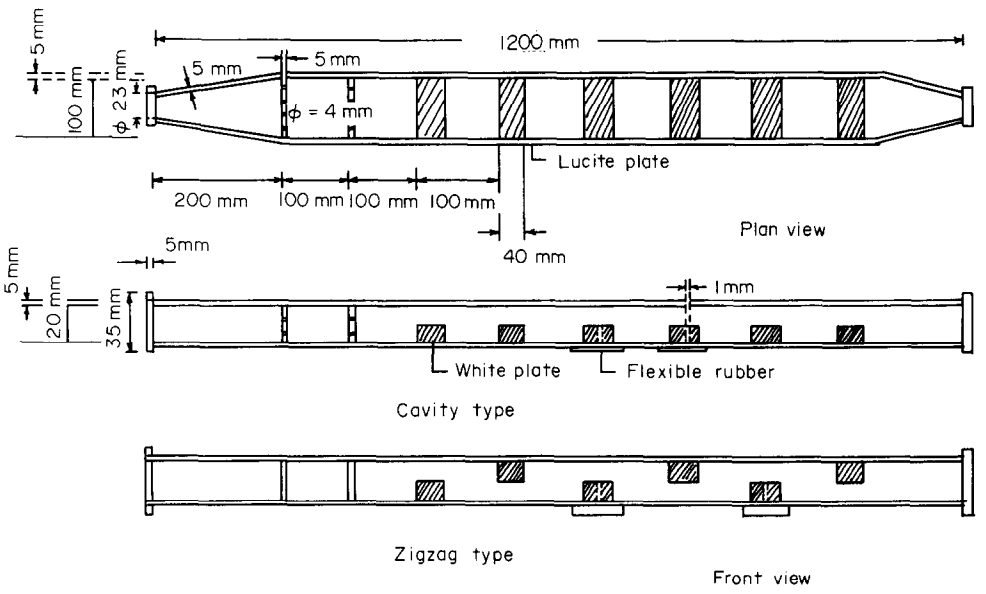

FIG. 8. Details of the experimental cells for flow visualization.

using 67 × 21 nodes (relative difference: 3–9%, average 4.5% for $Re = 50$, 6.2% for $Re = 200$), the slopes are almost the same in both cases. Further tests by varying the number of nodes or by varying the Reynolds number were not performed due to the limitation of the computer available (HP 3000-II).

It should be recognized that the values of the exponents x, y for the zigzag-type promoters are not different from those of the correlations which have been obtained experimentally by previous workers [1, 3, 25, 26]. Most of them assumed that $x = 1/3$ and $y = 1/2$. Therefore it is evident that the present study provides the theoretical background for the experimental work of previous investigators and could be valuable when attempting to design a better turbulence promoter.

4. FLOW VISUALIZATION

4.1. *Experimental*

The flow visualization for promoters with the aspect ratio $A = 5$ is performed to find the streamline distributions and the eddy lengths in order to see whether the results of the numerical analysis are consistent with the experimental results. The details of the experimental cells are shown in Fig. 8. The tracer injection holes are located at the third or fourth promoter. In all experiments tap water at room temperature is used as the working fluid. Sky blue ink (Pilot, Korea) is used as the tracer.

The photographic system consists of a 20 W fluorescent lamp, a white back curtain and a camera (Nikon E12, Japan) with a close-up lens (Micro-Nikor 55/3.5, Japan). A low speed film (ASA 32) is used for the low range of the Reynolds numbers with a highly sensitive film (ASA 400) for higher Reynolds numbers.

4.2. *Results and discussion*

The main sequence of photographs in Figs. 9(a) and (b) shows the growth of the eddy behind the zigzag-type promoter and the transition to the turbulence. As predicted by the numerical analysis, eddies are also formed in front of the promoter in the third photograph of Fig. 9(b). It is found that the instability of the recirculating flow begins at Reynolds numbers of about $Re = 250$–300 in the form of small amplitude oscillations at the rear part of the eddy. A further increase in Reynolds number makes the flow more unstable and results in a transition to turbulence as shown in the last two photographs of Fig. 9(b).

For the cavity-type promoter two important characteristics of the recirculating flow predicted by the numerical analysis are demonstrated in Figs. 9(c) and (d): (i) two eddies coexist under the contour $\psi = 0$ at a Reynolds number of about 100 and there exists an intermediate region across which the flow direction is reversed. Only the $\psi = 0$ line can be observed in the photographs for $Re = 82$ and 100 in Fig. 9(d). (ii) The eddy center is located at the far right-hand part of the cavity and at a height of $y = 1/2$–$2/3$ of the cavity depth ($x \simeq 3.7$, $y \simeq 0.27$) for higher Reynolds numbers ($Re > 200$) as shown for $Re = 220$.

Figure 10 shows a quantitative comparison between the predicted eddy lengths and those measured experimentally. The flow visualization results are in good agreement with the numerical predictions at Reynolds numbers ranging from 20 to 150. The small deviation from the predicted curve is due to the mean velocity at the injection point being greater than the overall volume-averaged velocity used to calculate the Reynolds number [27]. The deviation for Reynolds numbers greater than 150 may be partly due to the artificial viscosity effect of the upwind difference scheme.

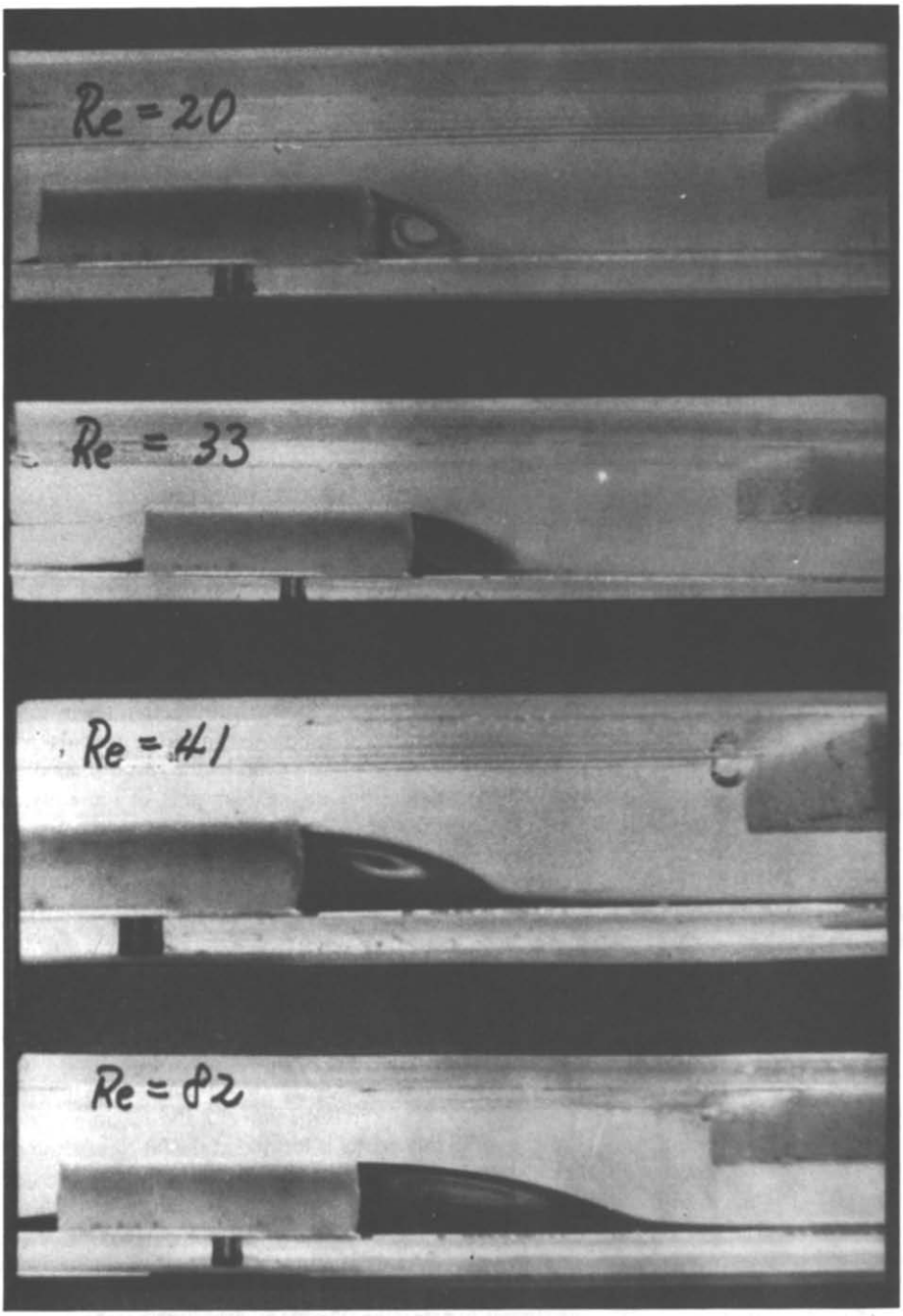

FIG. 9(a). Photographs for the zigzag-type promoters at $Re = 20$–82.

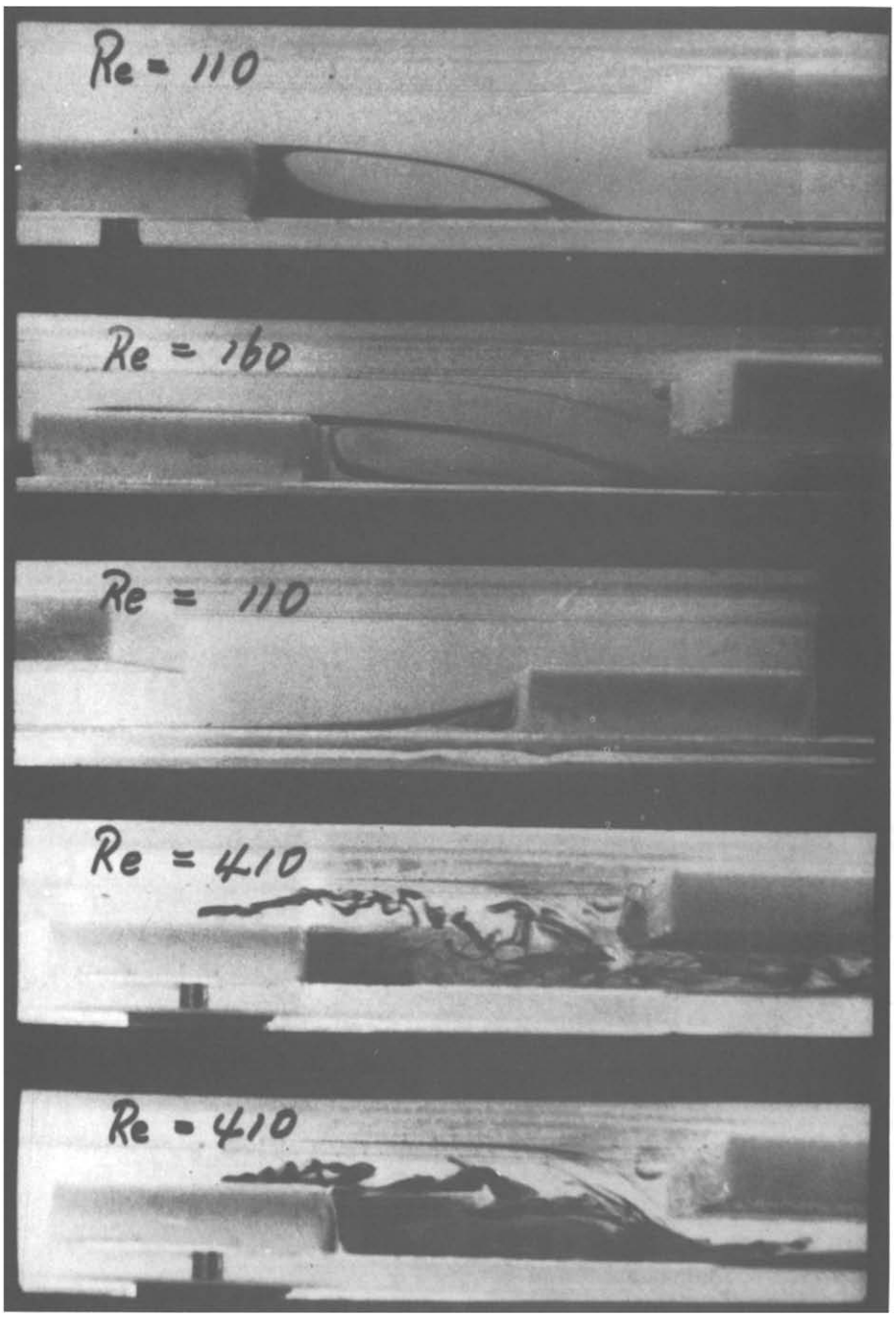

FIG. 9(b). Photographs for the zigzag-type promoters at $Re = 110$–410.

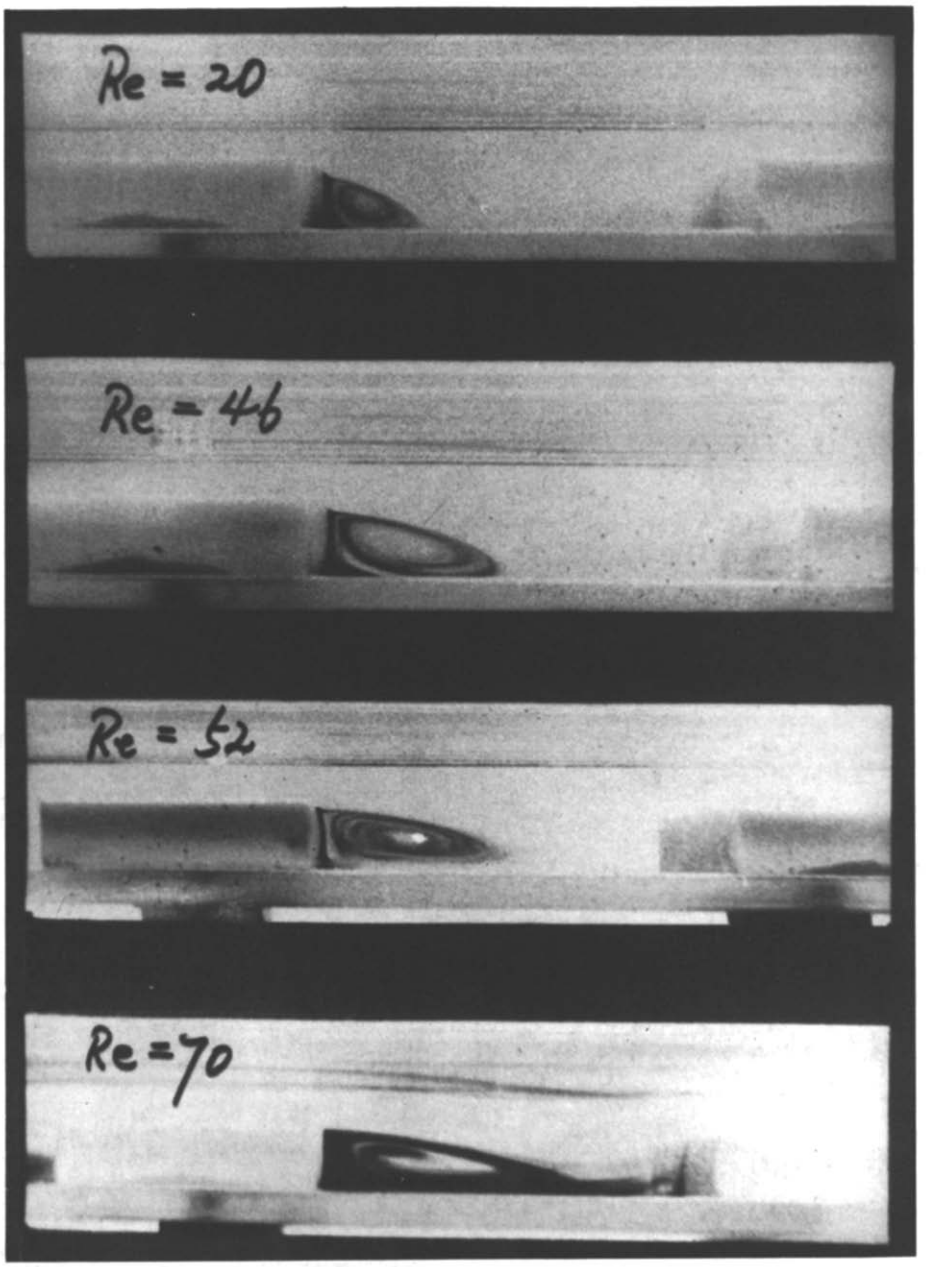

FIG. 9(c). Photographs for the cavity-type promoters at $Re = 20$–70.

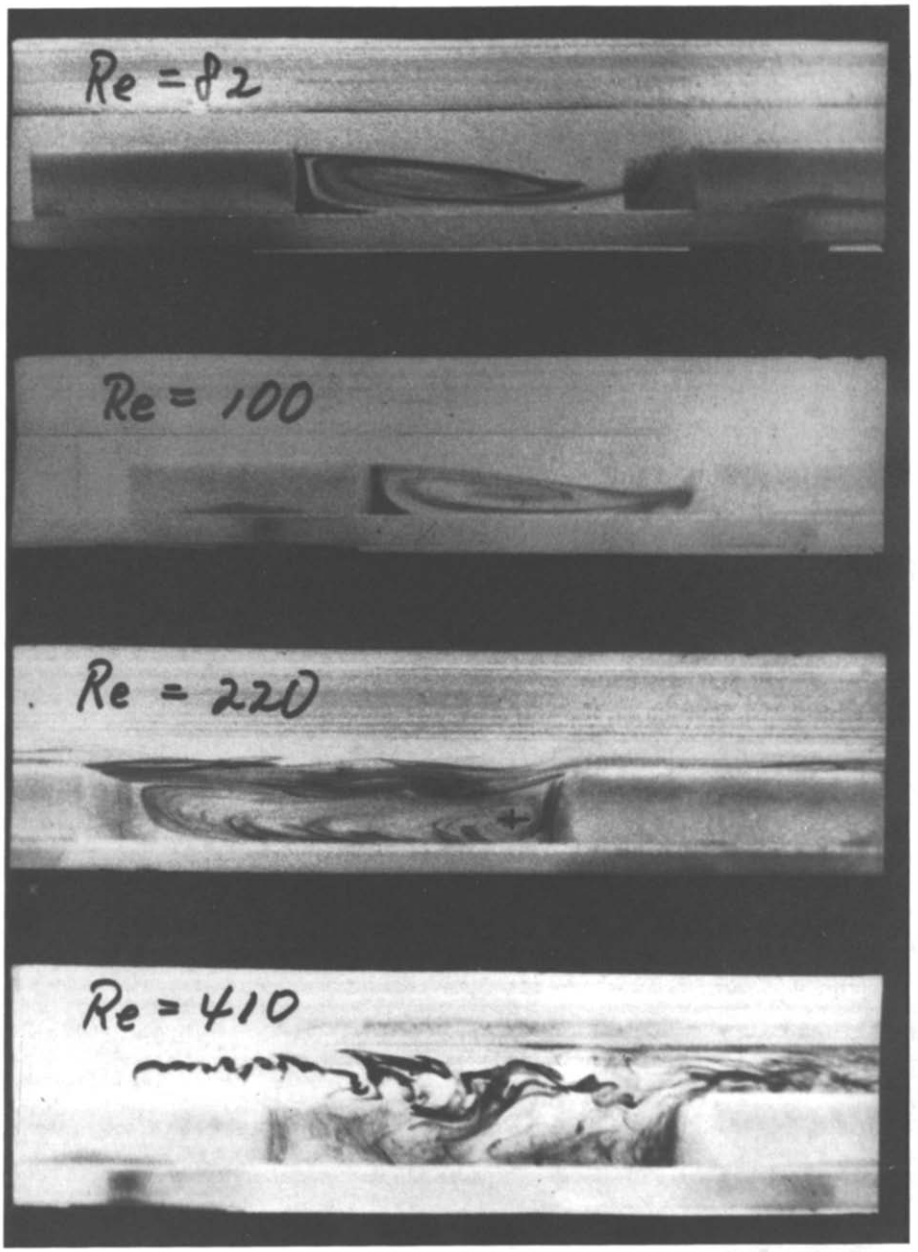

FIG. 9(d). Photographs for the cavity-type promoters at $Re = 82$–410.

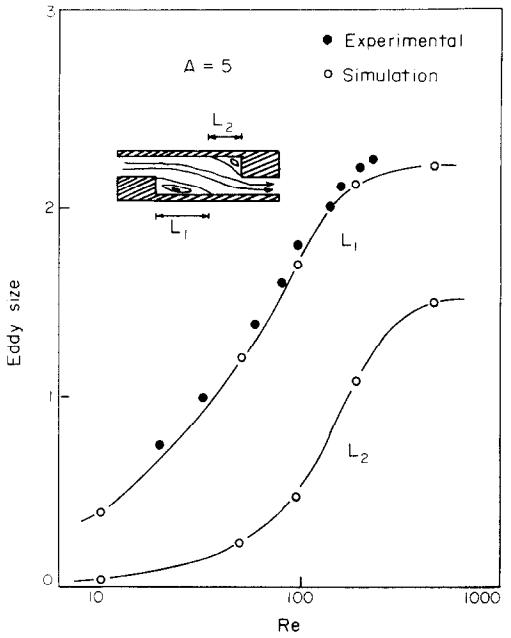

FIG. 10. Comparison of the calculated eddy sizes and the experimental values.

5. CONCLUSIONS

Careful examination of the solutions obtained shows that turbulence promoters enhance the mass transfer by forming a recirculating flow which gives the convective mass transfer effect and increases the wall shear stress in the main stream. Also they show that local Sherwood number distributions are closely related to the convective mass transfer and the wall shear stress distributions.

The following empirical correlations are obtained for the mass transfer of the promoters with the aspect ratio $A = 5$:

zigzag-type promoter $Sh = 0.519\, Sc^{0.376}\, Re^{0.475}$

cavity-type promoter $Sh = 1.069\, Sc^{0.376} Re^{0.294}$

The flow separations shown by flow visualization are in good agreement with the predictions by numerical analysis at Reynolds numbers from 20 to 150. Also the visualization studies show that the unsteady flow begins at Reynolds numbers of 250–300 for both types of geometries ($A = 5$).

Acknowledgements—The authors are indebted to the Korea Science and Engineering Foundation for partial support of this research. The authors are grateful to one of the referees for the suggestion of alternative boundary conditions for solving this problem.

REFERENCES

1. M. S. Isaacson and A. A. Sonin, Sherwood number and friction correlations for electrodialysis systems with application to process optimization, *I/EC Process Des. Dev.* **15**, 313–321 (1976).
2. G. Belfort and G. A. Gutter, An experimental study of electrodialysis hydrodynamics, *Desalination* **10**, 221–262 (1972).
3. Y. Winograd, A. Solan and M. Toren, Mass transfer in narrow channels in the presence of turbulence promoters, *Desalination* **13**, 171–186 (1973).
4. J. K. Aggarwal and L. Talbot, Electrochemical measurements of mass transfer in semi-cylindrical hollows, *Int. J. Heat Mass Transfer* **22**, 61–75 (1979).
5. D. Moalem-Maron, S. Sideman and H. Horn, Enhanced film mass transfer coefficients on grooved horizontal conduits, *Chem. Engng Sci.* **34**, 420–425 (1979).
6. C. B. Thorsness and T. J. Hanratty, Mass transfer between a flowing fluid and a solid wavy surfaces, *A.I.Ch.E. Jl* **25**, 686–697 (1979).
7. G. K. Batchelor, A proposal concerning laminar wakes behind a bluff at large Reynolds numbers, *J. Fluid Mech.* **1**, 388–398 (1956).
8. O. R. Burggraf, Analytical and numerical studies of structure of steady separated flows, *J. Fluid Mech.* **24**, 113–151 (1966).
9. E. E. Cormack and L. G. Leal, Natural convection in a shallow cavity with differentially heated walls, *J. Fluid Mech.* **65**, 209–230 (1974).
10. J. L. Duda and J. S. Vrentas, Heat transfer in a cylindrical cavity, *J. Fluid Mech.* **45**, 261–279 (1971).
11. K. S. Walker and G. M. Homsy, Convection in a porous cavity, *J. Fluid Mech.* **81**, 449–474 (1978).
12. W. F. Ames, *Numerical Methods for Partial Differential Equations*. Barness & Noble, New York (1969).
13. A. A. Gosman, W. M. Pun, A. K. Runchal, D. B. Spalding and M. Wolfshtein, in *Heat and Mass Transfer in Recirculating Flows*. Academic Press, London (1969).
14. A. Hadjidimos, Accelerated over-relaxation method, *Math. Comp.* **32**, 149–157 (1978).
15. M. Ikegawa, A new finite element technique for the analysis of steady viscous flow problems, *Int. J. Num. Methods Engng* **14**, 103–113 (1979).
16. A. Moult, D. Burley and H. Rawson, The numerical solution of two dimensional steady flow problems by the finite element method, *Int. J. Num. Methods Engng* **14**, 11–35 (1979).
17. M. Nallasamy and P. K. Krishina, Numerical studies on quasilinear and linear elliptic equations, *J. Comp. Phys.* **15**, 429 (1974).
18. M. Nallasamy and P. K. Krishina, On cavity flow at high Reynolds numbers, *J. Fluid Mech.* **79**, 391–414 (1977).
19. F. Pan and A. Acrivos, Steady flows in rectangular cavities, *J. Fluid Mech.* **28**, 643–655 (1967).
20. M. A. Lamb, *Hydrodynamics* (6th edn.). Dover, New York (1945).
21. J. S. Newman, *Electrochemical Systems*. Prentice-Hall, Englewood Cliffs (1973).
22. N. Mitchell, in *Heat and Mass Transfer in Recirculating Flows*. Academic Press, London (1969).
23. M. Schlichting, *Boundary Layer Theory* (6th edn.). McGraw-Hill, New York (1968).
24. C. S. Yih, *Fluid Mechanics*. McGraw-Hill, New York (1969).
25. R. E. Hicks and W. G. B. Mandersloot, The effect of viscous forces on heat and mass transfer in systems with turbulence promoters in packed beds, *Chem. Engng Sci.* **23**, 1201–1210 (1968).
26. A. A. Sonin and M. S. Isaacson, Optimization of flow design in forced flow electrochemical systems, *I/EC Process Des. Dev.* **13**, 241–248 (1974).
27. J. M. McKelvey, *Polymer Processing*. John Wiley, New York (1962).

EFFET DES PROMOTEURS DE TURBULENCE SUR LE TRANSFERT MASSIQUE-ANALYSE NUMERIQUE ET VISUALISATION DE L'ECOULEMENT

Résumé—Des études numériques sont faites sur le transfert massique dans un écoulement bidimensionnel entre deux plaques parallèles avec des promoteurs de turbulence placés sur la paroi inférieure et/ou supérieure. Les géométries de type "zigzag" et "cavité" sont choisies pour conduire les études de transfert massique et de visualisation d'écoulement dans le régime laminaire. Les résultats numériques montrent que les promoteurs de turbulence augmentent le transfert massique en formant un écoulement de recirculation qui donne l'effet de convection massique et accroît la contrainte pariétale de frottement.

Les séparations d'écoulement observées par visualisation sont en bon accord avec les calculs numériques pour des nombres de Reynolds allant de 20 à 150. La visualisation montre aussi que l'écoulement non stationnaire dans le canal commence à un nombre de Reynolds entre 250 et 300 pour les deux types de géométrie avec un rapport de forme égal à 5.

STOFFTRANSPORT—NUMERISCHE BERECHNUNG UND STRÖMUNGSBEOBACHTUNG

Zusammenfassung—Es wurden numerische Untersuchungen über den Stofftransport in einer zweidimensionalen Strömung zwischen zwei parallelen Platten mit Turbulenzerzeugern, die an der oberen und/oder an der unteren Wand angebracht waren, durchgeführt. "Zickzack"- und "Taschen"- Geometrien wurden für Untersuchungen des Stofftransports, verbunden mit Strömungsbeobachtungen, im laminaren Strömungsbereich ausgewählt. Die numerischen Ergebnisse zeigen, daß die Turbulenzerzeuger den Stofftransport erhöhen. Dies ist auf die sich ausbildende Rezirkulationsströmung, welche Einfluß auf den konvektiven Stofftransport hat und eine Erhöhung der Wandschubspannung in der Hauptströmung ergibt, zurückzuführen. Die bei den Beobachtungen festgestellten Strömungsablösungen sind für Reynolds-Zahlen von 20 bis 150 in guter Übereinstimmung mit den Ergebnissen aus den numerischen Berechnungen. Die Beobachtungen zeigen auch, daß für beide Geometrien bei Teilungsverhältnissen von 5 und für Reynolds-Zahlen ab 250 bis 300 eine unregelmäßige Strömung im Kanal entsteht.

ВЛИЯНИЕ ТУРБУЛИЗАТОРОВ НА МАССОПЕРЕНОС. ЧИСЛЕННЫЙ АНАЛИЗ И ВИЗУАЛИЗАЦИЯ ПОТОКА

Аннотация — Проведены численные исследования массопереноса при двумерном течении между двумя параллельными пластинами с турбулизаторами, прикрепленными к нижней и (или) верхней пластине. Использовались каналы в форме «зигзаг» или «полость», в которых исследование массопереноса и визуализация потока проводились в режиме ламинарного течения. Численные результаты показывают, что турбулизаторы способствуют усилению массопереноса за счет образования обратного течения, которое вызывает конвективный массоперенос и увеличивает касательное напряжение на стенке.

Наблюдаемая отрывная зона хорошо согласуется с результатами расчетов, проведенных при значениях числа Рейнольдса от 20 до 150. Кроме того, показано, что для двух типов геометрий канала при значениях числа Рейнольдса от 250 до 300 возникает нестационарность течения.